Blackbody components in gamma-ray bursts spectra?

G. Ghirlanda, Z. Bosnjak, G. Ghisellini, F. Tavecchio, C. Firmani

Mon. Not. R. Astron. Soc. **379,** 73–85 (2007) doi:10.1111/j.1365-2966.2007.11890.x

Blackbody components in gamma-ray bursts spectra?

G. Ghirlanda,[1⋆] Z. Bosnjak,[1,2] G. Ghisellini,[1] F. Tavecchio[1] and C. Firmani[1,3]

[1]*Osservatorio Astronomico di Brera, via E. Bianchi 46, I-23807 Merate, Italy*
[2]*Institut d'Astrophysique de Paris, 98 bis bd Arago, 75014 Paris, France*
[3]*Instituto de Astronomía, U.N.A.M., A.P. 70-264, 04510, México, D.F., México*

Accepted 2007 April 20. Received 2007 April 20; in original form 2007 February 13

ABSTRACT

We study seven gamma-ray bursts (GRBs), detected both by the Burst And Transient Source Experiment (BATSE) instrument, onboard the *Compton Gamma-ray Observatory*, and by the Wide Field Camera (WFC), onboard *BeppoSAX*. These bursts have measured spectroscopic redshifts and are a sizeable fraction of the bursts defining the correlation between the peak energy $E_{\rm peak}$ (i.e. the peak of the νF_ν spectrum) and the total prompt isotropic energy $E_{\rm iso}$ (so-called 'Amati' relation). Recent theoretical interpretations of this correlation assume that blackbody emission dominates the time-resolved spectra of GRBs, even if, in the time-integrated spectrum, its presence may be hidden by the change of its temperature and by the dilution of a possible non-thermal power-law component. We perform a time-resolved spectral analysis and show that the sum of a power law and a blackbody gives acceptable fits to the time-dependent spectra within the BATSE energy range but overpredicts the flux in the WFC X-ray range. Moreover, a fit with a cut-off power law plus a blackbody is consistent with the WFC data but the blackbody component contributes a negligible fraction of the total flux. On the contrary, we find that fitting the spectra with a Band model or a simple cut-off power-law model yields an X-ray flux and spectral slope which well matches the WFC spectra.

Key words: radiation mechanisms: non-thermal – radiation mechanisms: thermal – gamma-rays: bursts.

1 INTRODUCTION

Our knowledge of the spectral properties of the prompt emission of long gamma-ray bursts (GRBs) is based on systematic studies of their time-integrated spectrum (e.g. Golenetskii et al. 1983; Band et al. 1993; Amati et al. 2002; Barraud et al. 2003) which turned out to be described by two smoothly joint power laws with typical photon indices $\alpha \simeq -1$ and $\beta \simeq -2.5$ for the low- and high-energy components, respectively, or a cut-off power law (CPL). Several studies aiming to characterize the time-dependent behaviour of the spectrum (Ford et al. 1995; Crider, Liang & Smith 1997; Preece 1997; Ryde & Svensson 2000; Ghirlanda, Celotti & Ghisellini 2002; Kaneko et al. 2006) have demonstrated that the overall spectral shape and the peak energy $E_{\rm peak}$ [in a $\nu F(\nu)$ plot] evolve in time. The evolution is rather complex and there is no unique trend, but a prevalence of a hard-to-soft behaviour is observed.

The time-integrated properties, however, are the ones used to calculate the bolometric emitted energy of GRBs (both isotropic, $E_{\rm iso}$, and collimation corrected, E_γ) and to relate them to the peak energy $E_{\rm peak}$ (the so-called 'Amati', 'Ghirlanda' and 'Liang & Zhang' relations – Amati et al. 2002; Ghirlanda, Ghisellini & Lazzati 2004, hereafter GGL04; Liang & Zhang 2005; Ghirlanda et al. 2007). Furthermore, even the correlation between the isotropic peak luminosity $L_{\rm peak}$ and $E_{\rm peak}$ (the so-called 'Yonetoku' relation; Yonetoku et al. 2004) and the $L_{\rm peak} - E_{\rm peak} - T_{0.45}$ relation (the so-called 'Firmani' relation; Firmani et al. 2006) makes use of the time-integrated spectrum (see Ghirlanda et al. 2005). The fact that these correlations apply to the time-integrated spectrum, even if it evolves in time, may underline some global property of the burst.

In this respect, there have been, very recently, important suggestions and new ideas for explaining the 'Amati', the 'Ghirlanda' and also the 'Firmani' relation. The simplest way to have a relation between the emitted energy or luminosity and $E_{\rm peak}$ is through blackbody emission. Indeed, in this case, the number of free parameters is kept to a minimum: the rest-frame bolometric and isotropic blackbody luminosity would depend on the emitting surface, the temperature and the bulk Lorentz factor. Any other emission process would depend on some extra parameters, such as the magnetic field and/or the particle density, and it would then be more difficult, if these quantities vary from burst to burst, to produce a correlation with a relatively small scatter such as the $E_{\rm peak} - E_\gamma$ one.

Rees & Meszaros (2005), Thompson (2006) and Thompson, Meszaros & Rees (2006) explain these correlations assuming that a considerable fraction of the prompt emission flux is due to a blackbody. This does not imply, however, that the entire observed

⋆E-mail: giancarlo.ghirlanda@brera.inaf.it

flux is a single blackbody (we already know that this is not the case).

Indeed, time-integrated GRB spectra are typically described by the Band (B) model or CPL model. The time-integrated spectrum, however, being the result of the spectral evolution, could be best fitted by a model which is not the same used for the time-resolved spectra. Within the blackbody interpretation, there could be at least two alternatives: the time-integrated spectrum (which looks like a CPL or a B model) is (a) the result of the superposition of different blackbodies with a time-dependent temperature and flux or (b) the sum of two components, i.e. one thermal (blackbody) and one non-thermal (power law or double power law) as suggested by Ryde (2004). In both the cases, since the temperature of the single (time-resolved) blackbodies and/or the slope of the power law can evolve in time, the time-integrated spectrum could well be modelled by a smoothly broken power law (i.e. the Band function, see below), hiding the presence of the blackbody. This requires to perform the time-resolved spectral analysis in order to assess the presence of an evolving blackbody component possibly with a non-thermal power-law component.

Evidence of the presence of a thermal blackbody component was discovered in the BATSE spectra [e.g. Ghirlanda, Celotti & Ghisellini (2003), hereafter GCG03]. This component dominates the initial emission phase up to ∼2 s after the trigger. During this phase, the luminosity and the temperature evolve similarly in different GRBs while the late time spectrum is dominated by a non-thermal component (e.g. it is fitted with the empirical Band et al. 1993 model). Attempts to deconvolve these spectra with a mixed model, i.e. a blackbody plus a power law (Ryde 2005), showed that the blackbody (albeit with a monotonically decreasing flux) could also be present during later phases of the prompt emission (see also Bosnjak et al. 2006).

As a test of the recently proposed 'blackbody' interpretations of the $E_{\rm peak}-E_{\rm iso}$ and $E_{\rm peak}-E_{\gamma}$ correlations, we consider, among the sample of GRBs used to define these correlations, those bursts that were detected by BATSE and with published Wide Field Camera (WFC) spectra. Given the relatively large brightness of these bursts, it is possible for them to meaningfully analyse the time-dependent properties of their spectra.

The focus of this paper is not much on the study of the spectral evolution of these few bursts,[1] but, instead, on the relevance of the blackbody in the time-resolved spectra together with the relevance of the sum of the blackbodies, possibly at different temperatures, in the time-integrated spectrum. To this aim, we adopt for our analysis a power-law+blackbody model, besides the 'standard' B and CPL model. We anticipate that the power-law+blackbody model, although giving acceptable fits, is inconsistent with the WFC data. A more complex fit, made by adopting the sum of a blackbody and a CPL, is equally acceptable and consistent with the WFC data, but implies that the blackbody flux is a minor fraction of the total.

The paper is organized as follows. In Section 2, we recall the basic ideas of the 'blackbody' interpretation of the $E_{\rm peak}-E_{\rm iso}$ and $E_{\rm peak}-E_{\gamma}$ correlations; in Section 3 we introduce the sample and the spectral analysis procedure, and present the results of the time-resolved spectral analysis and the comparison of the BATSE and WFC spectra with the three adopted model. We discuss our results in Section 4.

[1]The analysis of how the spectral parameters evolve in time with respect to the $E_{\rm peak}-E_{\rm iso}$ and $E_{\rm peak}-E_{\gamma}$ correlations is the content of a forthcoming paper (Bosnjak et al., in preparation).

2 THE INTERPRETATION OF THE SPECTRAL-ENERGY CORRELATIONS

The recent theoretical attempts to explain the spectral-energy relations, and in particular the $E_{\rm peak}-E_{\rm iso}$ (Amati) one, largely motivate the present work. Therefore, it may be useful to summarize here the arguments put forward by Thompson (2006) and by Thompson et al. (2006).

Consider a fireball that at some distance R_0 from the central engine is moving relativistically with bulk Lorentz factor Γ_0. As an example, one can think that R_0 is the radius of the progenitor star. Assume that a large fraction of the energy that the fireball dissipates at R_0 is thermalized and forms a blackbody of luminosity:

$$L_{\rm BB,iso} = \pi R_0^2 \Gamma_0^2 \sigma T_0'^4 = \pi \frac{R_0^2}{\Gamma_0^2} \sigma T_0^4, \quad (1)$$

where T_0' and $T_0 = \Gamma_0\, T_0'$ are the temperatures at R_0 in the comoving and observing frame, respectively. The collimation corrected luminosity is $L_{\rm BB} = (1-\cos\theta_{\rm j}) L_{\rm BB,iso}$, which, for small semi-aperture angles of the jetted fireball (assumed to be conical), gives

$$\theta_{\rm j}^2 \sim \frac{2 L_{\rm BB}}{L_{\rm BB,iso}}. \quad (2)$$

Now, Thompson (2006) and Thompson et al. (2006) introduce one key assumption: for causality reasons $\Gamma_0 \sim 1/\theta_{\rm j}$. This allows to substitute Γ_0 in equation (1) to obtain

$$L_{\rm BB,iso} \sim 2\pi R_0^2 \frac{L_{\rm BB}}{L_{\rm BB,iso}} \sigma {T_0}^4. \quad (3)$$

Setting $E_{\rm BB,iso} = L_{\rm BB,iso} t_{\rm burst}$ and $E_{\rm BB} = L_{\rm BB} t_{\rm burst}$, where $t_{\rm burst}$ is the duration of the prompt emission, one has

$$E_{\rm peak} \propto T_0 \propto E_{\rm BB,iso}^{1/2} E_{\rm BB}^{-1/4} t_{\rm burst}^{-1/4}. \quad (4)$$

This reproduces the 'Amati' relation if $E_{\rm BB}$ is nearly the same in different bursts and if the dispersion of the GRB duration is not large. One can see that a key assumption for this derivation is the blackbody law. It is the $L \propto T^4$ relation which allows to derive $E_{\rm peak} \propto E_{\rm iso}^{1/2}$.

3 SAMPLE SELECTION AND ANALYSIS

We consider all bursts detected by BATSE with measured spectroscopic redshift which were also detected by *BeppoSAX* and for which the WFC data were published (Frontera, Amati & Costa 2000; Amati et al. 2002). In Table 1, we list our bursts and their time-integrated spectral properties as found in the literature. We also report the duration (T_{90}) derived from the BATSE gamma-ray light curve, the 50–300 keV energy fluence and the hard X-ray (2–28 keV) energy fluence. We also include in our sample GRB 980329 and 980326 for which only a range of possible redshifts (the most accurate for 980326) were found (see also GGL04).

For all the bursts, we analysed the BATSE Large Area Detector (LAD) spectral data which consist of several spectra accumulated in consecutive time bins before, during and after the burst. Only for GRB 990123, we analysed the Spectroscopic Detectors (SD) data because of a gap in the LAD data sequence. The spectral analysis has been performed with the software SOAR V3.0 [Spectroscopic Oriented Analysis Routines by Ford (1993)], which we implemented for our purposes.

For each burst, we analysed the BATSE spectrum accumulated over its total duration (which in most cases corresponds to the T_{90} parameter reported in the BATSE catalogue) and the time-resolved

Table 1. Time-integrated properties of the bursts with spectroscopic redshift and detected by both BATSE and *BeppoSAX* and with published *BeppoSAX*-WFC spectra. The duration T_{90} and the (50–300 keV) fluence [F(50–300 keV)] are from the online BATSE catalogue. The 2–28 keV fluence is reported from table 1 of Amati et al. (2002) for all bursts except GRB 980425 for which we report the 2–26 keV fluence given in Pian et al. (2000). In the case of GRB 980326, we could not find these information in the publicly available archive. For GRB 970508, we report the spectral results of the *BeppoSAX* data (first line) and the results obtained from the BATSE data (second line). First set of references is for the redshift: (1) Metzger et al. (1997); (2) Kulkarni et al. (1998); (3) Bloom et al. (1999); (4) Lamb, Castander & Reichart (1999) (and references therein); (5) Galama et al. (1998); (6) Kulkarni et al. (1999); (7) Vreeswijk et al. (2001); Second set of references is for the spectral parameters: (8) Amati et al. (2002) and (9) Jimenez, Band & Piran (2001).

GRB	z	α	β	$E_{\rm peak}$ (keV)	References	T_{90} (s)	F(50–300 keV) (erg cm^{-2})	F(2–28 keV) (erg cm^{-2})
970508	0.835	−1.71 (0.1)	−2.2 (0.25)	79 (23)	1, 8			
	0.835	−1.19	−1.83	>1800	1, 9	23.1 ± 3.8	1.1×10^{-6}	8.3×10^{-7}
971214	3.418	−0.76 (0.1)	−2.7 (1.1)	155 (30)	2, 8	31.23 ± 1.18	6.44×10^{-6}	3.2×10^{-7}
980326	0.9–1.1	−1.23 (0.21)	−2.48 (0.31)	33.8 (17)	3, 8	...	...	5.5×10^{-7}
980329	2–3.9	−0.64 (0.14)	−2.2 (0.8)	233.7 (37.5)	4, 8	18.56 ± 0.26	3.2×10^{-5}	4.3×10^{-6}
980425	0.0085	−1.26		120	5, 9	34.88 ± 3.78	2.47×10^{-6}	1.8×10^{-6}
990123	1.6	−0.89 (0.08)	−2.45 (0.97)	781 (62)	6, 8	63.4 ± 0.4	1.0×10^{-4}	9.0×10^{-6}
990510	1.602	−1.23 (0.05)	−2.7 (0.4)	163 (16)	7, 8	68 ± 0.2	1.1×10^{-5}	5.5×10^{-6}

spectra distributed within this time interval. The time-resolved spectra are accumulated onboard according to a minimum signal-to-noise criterion with a minimum integration time of 128 ms. As the bursts of our sample have quite large fluence (i.e. $\geqslant 10^{-6}$ erg cm^{-2} integrated over the 50–300 keV range) in most cases we could analyse their time-resolved spectra as they were accumulated by the onboard algorithm. Only the spectra at the beginning or at the end of the bursts (or during interpulses phases) were accumulated in time in order to have a larger signal. Energy rebinning [i.e. at least 30 (15) counts per bin for the LAD (SD) spectra] was systematically applied in our analysis in order to test the goodness of the fits through the χ^2 statistics.

The adopted spectral analysis procedure is the standard forward-folding which folds the model spectrum with the detector response and, by varying the model-free parameters, minimizes the χ^2 between the model and the data. This procedure requires the knowledge of the background spectrum corresponding to each analysed spectrum. In order to account for the possible time variability of the background, we modelled it as a function of time. We selected two time intervals (before and after the burst) as close as possible to the burst (not contaminated by the burst itself) of typical duration 1000 s. We fit the spectra contained in these intervals with a background model which is a polynomial function of time $B(E, t)$, and, being a spectrum, also of the energy E. Each energy bin of the spectra selected for the background calculation is interpolated with this polynomial function. This fit is tested for by inspecting the distribution of its χ^2 as a function of energy. In this way, we obtain the best-fitting time-dependent background model function $B_{\rm best}(E, t)$ which is extrapolated to the time interval Δt of each time-resolved spectrum and subtracted to the data. This method is the same adopted in previous analysis of the BATSE data (e.g. Preece et al. 2000; Kaneko et al. 2006).

3.1 Spectral models

For the analysis of both the time-resolved and the time-integrated spectra, we use three models which were already tested in fitting the BATSE spectral data (Preece et al. 2000; Ghirlanda et al. 2002; Ryde 2004; Kaneko et al. 2006):

(i) The B model (originally proposed by Band et al. 1993) which consists of two power laws joined smoothly by an exponential roll-over. Its analytical form is

$$N(E) = AE^{\alpha} \exp\left(-\frac{E}{E_0}\right); \quad \text{for } E \leqslant (\alpha - \beta)\, E_0$$
$$N(E) = AE^{\beta}[(\alpha - \beta)E_0]^{\alpha-\beta} \exp(\beta - \alpha); \quad \text{for } E \geqslant (\alpha - \beta)\, E_0. \tag{5}$$

The free parameters, which are the result of the fit to the observed spectrum, are the normalization of the spectrum A; the low-energy power-law photon spectral index α; the high-energy power-law photon spectral index β and the break energy, which represents the e-folding parameter, E_0. If $\beta < -2$ and $\alpha > -2$, this model has a peak in the EF_E representation which is $E_{\rm peak} = (\alpha + 2)E_0$. In the fits, we assume that α and β can vary within the range $[-5, 1]$ while the break energy is allowed to vary in the same range covered by the spectral data, i.e. ∼30–1800 keV. The B model is a fair representation of the spectral model produced in the case of emission from a relativistic population of electrons, distributed in energy as a single or a broken power law, emitting synchrotron and/or inverse Compton radiation, and can also reproduce the case of an electron energy distribution which is a Maxwellian at low energies and a power law at high energies, emitting synchrotron radiation (e.g. Tavani 1996).

(ii) The CPL is composed by a power law ending-up in an exponential cut-off. It corresponds to the previous B model without the high-energy power-law component. Its form is

$$N(E) = AE^{\alpha} \exp\left(-\frac{E}{E_0}\right). \tag{6}$$

The free parameters are the same of the B model without the high-energy component. If $\alpha > -2$, this model also presents a peak in its EF_E representation which is $E_{\rm peak} = (\alpha + 2)E_0$. This model can represent the case of thermal or quasi-thermal Comptonization, even when saturated (i.e. a Wien spectrum, with $\alpha = 2$).

(iii) The blackbody + power-law (BBPL) model is

$$N(E) = A\frac{E^2}{\exp(E/kT) - 1} + BE^{\alpha}, \tag{7}$$

where α is the spectral index of the power law; kT the blackbody temperature and A and B the normalizations of the two spectral components. In this case, the peak of the νF_ν spectrum depends on the relative strength of the two model components and on the spectral energy range where the spectrum is considered. The peak energy

of the blackbody component only is $E_{\rm peak,BB} = 3.93\ kT$ (in $\nu\ F_\nu$). The (simplest) physical rationale of this model is the possible different origin of the two components: the thermal blackbody emission could be photospheric emission from the fireball (e.g. Daigne & Mochkovitch 2000) while the power-law component might be the non-thermal emission from relativistic electrons accelerated above the photosphere at the classical internal shock radius (see also Pe'er, Meszeros & Rees 2006). The BBPL model is the simplest spectral model which combines a thermal and a non-thermal component. In Section 5, we will also discuss the more complex case of a CPL plus a blackbody component.

Note that the number of free parameters is the same (i.e. four, including normalizations) in the B and BBPL model while the CPL model has one less free parameter.

The BATSE spectra were fitted in the past with all these models. Band et al. (1993) proposed the B function to fit the time-integrated spectra of bright, long GRBs. Also, the time-resolved spectra could be fitted by either the B or the CPL model (Ford et al. 1995; Ghirlanda et al. 2002). More recently, Kaneko et al. (2006) performed a systematic analysis of the time-resolved spectra of a large sample of BATSE bursts selected according to their peak flux and fluence. From these works, it results that the typical low-energy spectral slope (in both the B and CPL model) has a wide distribution centred around $\alpha \sim -1$ with no preference for any specific value predicted by the proposed emission models (i.e. $\alpha = -2/3$ for optically thin synchrotron – Katz 1994; $\alpha = -3/2$ for synchrotron cooling – Ghisellini & Celotti 1999; $\alpha = 0$ for jitter radiation – Medvedev 2000). The high-energy photon spectral index β has a similar dispersion (i.e. 0.25) of the α distribution and its typical value is -2.3. The peak energy has a narrow ($\sigma \leqslant 100$ keV) distribution centred at $\sim$300 keV. A small fraction (7 per cent) of the time-resolved spectra have $\beta > -2$ which means that the peak energy of the EF_E spectrum is above the upper energy threshold (i.e. $E_{\rm peak} > 2$ MeV). The composite BBPL model was fitted to the time-resolved spectra of a few bright BATSE bursts (Bosnjak et al. 2005; Ryde 2005).

In the following section, we present the spectral parameters of the fits obtained with the three models above. The scope of this paper is not to decide which (if any) of the proposed models best fit the spectra. It has been already shown (e.g. Ryde 2005) that the time-resolved BATSE spectra can be adequately fitted with both the B (CPL) model and the BBPL model.

4 RESULTS

Here, we show the spectral evolution and compare the spectral parameters of the three models described in Section 3. We also compare the spectral results of our analysis of the BATSE time-integrated spectra (reported in Table 2) with the results gathered from the literature (Table 1). We then discuss the contribution of the blackbody component to the spectrum and compare the spectral fits of the three models with the constraints given by the WFC data.

4.1 Spectral evolution

We present the spectral evolution of the fit parameters obtained with the three models described in Section 3.

4.1.1 GRB 970508

The spectral parameters of the time-integrated spectrum published in Amati et al. (2002) for GRB 970508 were found by the analysis of the WFC (2–28 keV) and gamma-ray burst monitor (GRBM, 40–700 keV) data and they differ from those found by the BATSE spectral analysis and those published in Jimenez et al. (2001). We report the different results in Table 1. The main difference is that according to the *BeppoSAX* spectrum, this burst has a considerably low peak energy while the BATSE spectrum indicates that $E_{\rm peak} > 1800$ keV. We have re-analysed the BATSE spectrum confirming the results found by Jimenez et al. (2000). In particular, we found an unconstrained peak energy when fitting both the B and the CPL model. The spectrum in the 40–700 keV energy range of GRB 970508 presented in Amati et al. (2002) is composed of only two data points with a quite large associated uncertainty. In this case, the fit (with the B model) is dominated by the WFC spectrum, which does not present any evidence of a peak (in νF_ν) within its energy range. Combining the GRBM and WFC data, Amati et al. (2002) found $E_{\rm peak} = 79$ keV, but the GRBM spectral data also appear consistent with a high-energy component with $\beta \geqslant -2$ (which is what is found from the fit of the BATSE spectrum). If the real GRB spectrum is that observed by BATSE, this burst would be an outlier for the Amati correlation (see also fig. 3 of GGL04). Given the possible uncertainties of the *BeppoSAX* spectrum, we do not consider this burst in the following analysis because the BATSE spectrum does not allow to constrain its peak energy.

Table 2. Time-integrated properties of the bursts of our sample. Spectral parameters were obtained from the analysis of the time-integrated spectrum of the BATSE data. We report the best-fitting model parameters. For GRB 990510, we give the spectral results of the first and the second emission episodes separately. Star (∗) represents that in these cases (see text) the reported χ^2_r (and the uncertainties associated to the spectral parameters) are without adding systematic errors to the fit (see text). $\alpha_{\rm PL}$ represents the photon spectral index of the power-law component of the BBPL model fitted to the time-integrated spectrum. $F_{\rm BB}$ represents the average of the blackbody contribution to the total flux obtained in the fits of the time-resolved spectra. In the final column, we show the contribution of the blackbody component when fitting a more complicated model (see text) composed by a CPL plus a blackbody. In these fits, the blackbody peak energy has been fixed to the value obtained by the fit of a simple CPL model. These results represent an upper limit to the blackbody component, i.e. obtained by forcing the blackbody to contribute to the peak of the spectrum. The reported blackbody percentage is obtained by integrating in time the single contribution obtained by the fit of the time-resolved spectra.

GRB	Model	α	β	$E_{\rm peak}$	χ^2_r	$\alpha_{\rm PL}$	% $F_{\rm BB}$	% $F_{\rm BB}^{\rm BBCPL}$
971214	CPL	−0.65 (0.1)	....	186 (15)	1.07	−1.9	36	23
980326	CPL	−1.21 (0.44)	...	65 (35)	1.02	−2.7	5	<1
980329	B	−0.93 (0.1)	−2.4(0.1)	253 (10)	1.6*	−1.7	30	26
980425	CPL	−1.26 (0.14)	...	123 (36)	1.04	−2.1	45	8
990123	B	−0.85 (0.04)	−2.44 (0.23)	607 (71)	1.04	−1.5	38	33
990510	CPL	−0.88(0.01)	...	92 (6)	1.3*	−2.12	32	1.3
	B	−1.16(0.05)	−2.28(0.06)	173(21)	1.5*	−1.92	18	13

4.1.2 GRB 971214

GRB 971214 (BATSE trigger 6533) has a highly variable light curve (Fig. 1, top panels) and the time-resolved spectral analysis could be performed on ∼20 s of the total GRB duration. In this time interval, we extracted 13 spectra. In Fig. 1, we show the time evolution of the spectral parameters for the B, CPL and BBPL model.

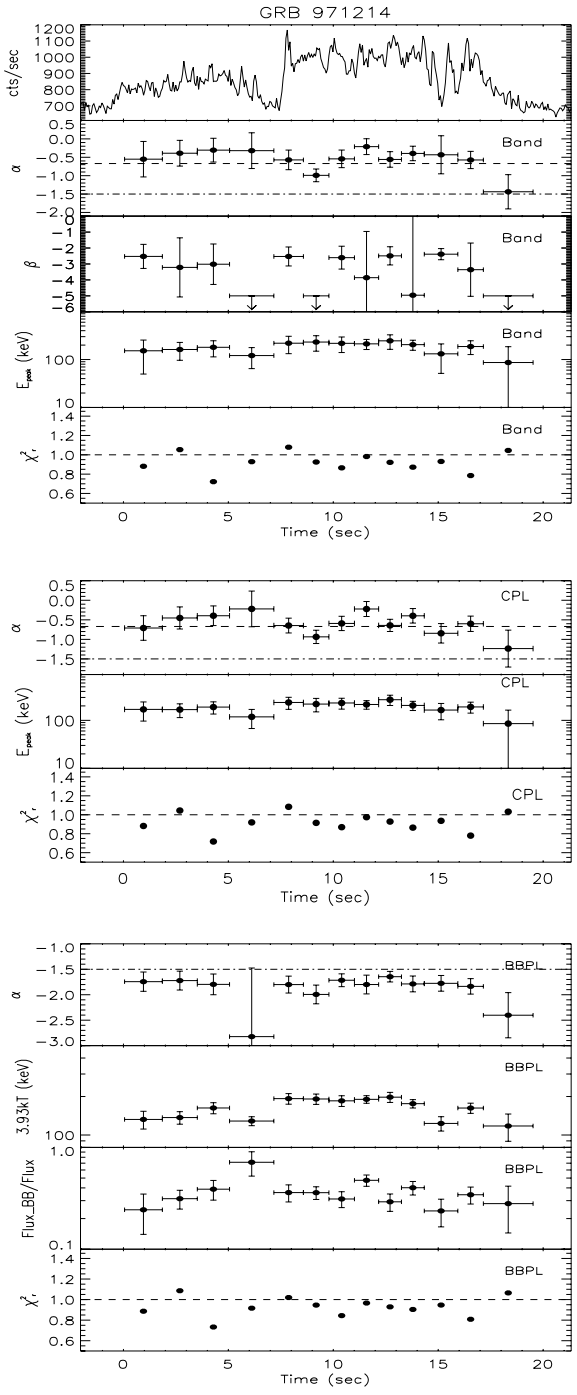

Figure 1. Spectral evolution of GRB 971214. Top panels: B model fit results. The first panel represents the light curve (in counts per second detected at energies ⩾25 keV – without the background subtraction). Mid panels: CPL fit results. Bottom panels: BBPL fit results (we also report the contribution of the blackbody component to the total flux in the observed 30 keV to 2 MeV energy range). For all the three models, we show for comparison the optically thin synchrotron limit ($\alpha = -2/3$, dashed lines) and the case of synchrotron cooling ($\alpha = -3/2$, dot–dashed line).

The low-energy spectral index α of the B and CPL model evolves similarly, and for most spectra this parameter violates the optically thin synchrotron limit (i.e. $\alpha = -2/3$; dashed line in Fig. 1) and, of course, the optically thin synchrotron limit in the case of radiative cooling (i.e. $\alpha = -3/2$; dot–dashed line in Fig. 1). In the case of the BBPL model instead, α is always consistent with (i.e. softer than) these limits and softer than the corresponding values found with the B or CPL model. The peak energy of the three models is very similar and tracks the light curve although it does not change dramatically. The BBPL fit shows that the peak energy of the blackbody component tracks the light curve. The blackbody can contribute up to ∼50 per cent of the total flux.

All the three models give acceptable fits for the time-integrated spectrum, accumulated over 20 s. The B model high-energy component is very soft (i.e. $\beta \sim 5$) making it consistent with the CPL model. For both these two models $\alpha \sim -0.66 \pm 0.08$ (1σ uncertainty; see Table 2), consistent with the value reported in Table 1 that was derived by fitting the WFC+GRBM *BeppoSAX* data (Amati et al. 2002).

4.1.3 GRB 980326

For GRB 980326 (BATSE trigger 6660), both the duration and the light curve are not available in the BATSE archive. By analysing the spectral evolution, we could extract only two spectra in approximately the total duration of the burst (∼5 s).[2] The first spectrum (from 0.09 to 1.56 s) is well fitted by the B and CPL models which give similar results, i.e. $\alpha = 1.2 \pm 0.3$, $\beta_B = -3.4 \pm 0.7$ and $E_{\rm peak} = 52 \pm 27$ keV, with $\chi^2_r = 0.93$ (for 102 degrees of freedom) and $\chi^2_r = 0.94$ (for 103 degrees of freedom) for the B and the CPL model, respectively. The second spectrum (from 1.56 to 4.09 s) has α and $E_{\rm peak}$ consistent with the first one. These two spectra, fitted with the BBPL model, show a soft power-law component (i.e. $\alpha_{\rm BBPL} \sim -2.5$) and peak energy of ∼74 keV (with $\chi^2_r = 1.0$).

The spectral parameters of the average spectrum of GRB 980326 are reported in Table 2 and they are consistent with those reported in Table 1. The only difference is the slightly larger value of $E_{\rm peak,B} \sim 65$ keV (with $\chi^2_r = 1.02$) obtained here.

4.1.4 GRB 980329

GRB 980329 (BATSE trigger 6665) has a structured light curve (Fig. 2, top panels) with at least two small peaks preceding two major peaks of similar intensity. For the spectral evolution, we could accumulate 37 time-resolved spectra within the ∼17 s duration of the burst corresponding to its T_{90}.

The low-energy spectral index α evolves similarly in the B and CPL model and its values are between the two synchrotron limits (i.e. $-2/3$ and $-3/2$). The fit with the BBPL model instead requires a very soft power-law component and a time evolution similar to that of the power-law index of both the B and CPL model, but with a value which is always smaller than $-3/2$.

The peak energy seems to evolve differently in the B and CPL model. In the B model, $E_{\rm peak}$ does not change much during the burst and remains below ∼300 keV, whereas in the CPL model $E_{\rm peak}$ changes in time and reaches ∼1 MeV in correspondence to

[2] This duration is consistent with the 9 s reported in table 1 of Amati et al. (2002), based on the *BeppoSAX* observation.

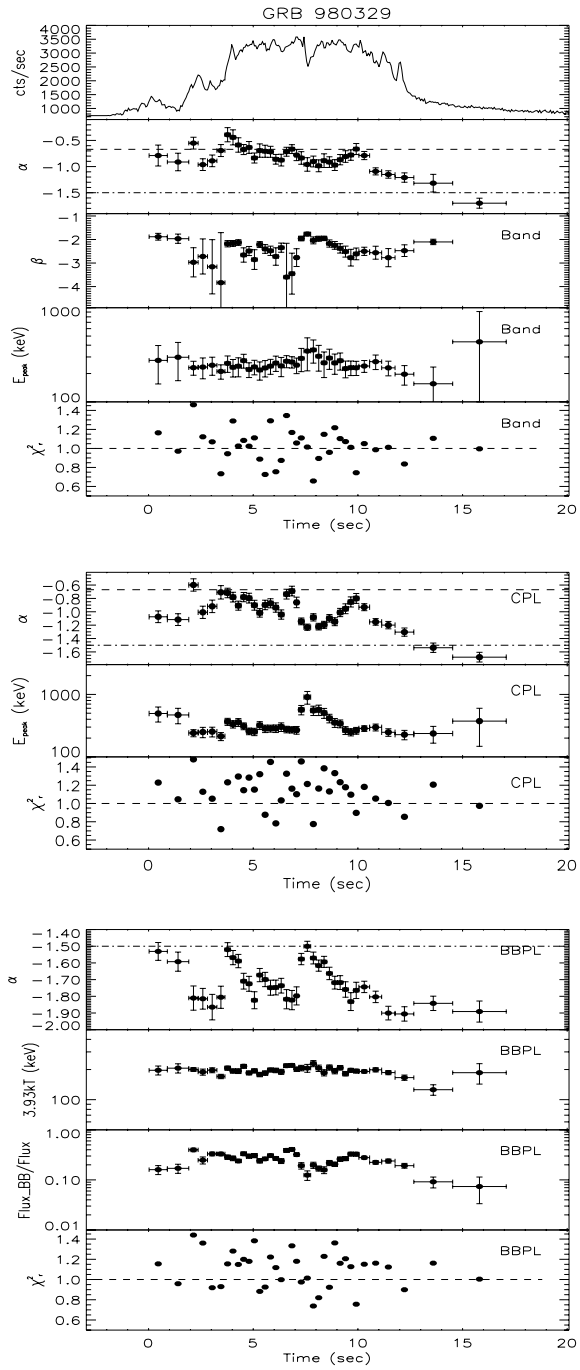

Figure 2. Spectral evolution of GRB 980329. Symbols are the same as in Fig. 1.

the major peak of the light curve (at 6 s). The fit with the BBPL model instead presents a peak energy which does not evolve much and, similarly to the B fit, stays constant at around 200 keV. The blackbody component contributes, at least, 40 per cent of the total flux (bottom panel in Fig. 2).

The average spectrum of GRB 980329 has been accumulated over its T_{90} and fitted with the three models. We found $\alpha = -0.93 \pm 0.1$, $\beta = -2.4 \pm 0.2$ and $E_{\rm peak} = 253 \pm 10$ keV (Table 2) for the fit with the B model. These spectral parameters are in good agreement (except for a softer low-energy spectral index) with those found by the fitting of the *BeppoSAX* data by combining the WFC/GRBM data (Amati et al. 2002) reported in Table 1. We note that a few time-resolved spectra of this burst and also the time-integrated spectrum have quite a large χ^2_r when fitted with all the three models. We suspect that this is due to the fact that these spectra are characterized by very small statistical errors. Indeed, we found that the use of 2 per cent of systematic errors uniformly distributed in the spectral range makes the fits acceptable. However, to the best of our knowledge, this has not been treated in the published literature. For this reason, we list the spectral results as they were obtained without accounting for additional systematic uncertainties. When accounting for systematic errors, the χ^2 improves, the fitted parameters remain unchanged and their associated uncertainties increase slightly.

4.1.5 GRB 980425

GRB 980425 (BATSE trigger 6707) is a long single-peaked smooth GRB famous for being the first GRB associated with a supernova (SN) event (i.e. SN1998bw – Galama et al. 1998). GRB 980425 is also the lowest redshift GRB ever detected. Due to its relatively low fluence, its isotropic equivalent energy is small compared to other bursts. Indeed, it is one of the two clear outliers (the other being GRB 031203) with respect to the $E_{\rm peak} - E_{\rm iso}$ correlation (but see Ghisellini et al. 2006).

With the aim of studying its spectral evolution, we extracted seven spectra during roughly 15 s. The time interval covered by our time-resolved spectral analysis is between the two durations T_{90} and $T_{50} = 9.79 \pm 0.29$ which, however, differs by a factor of 10. This limitation is due to the slow decay of the light curve after the trigger coupled to a relatively small intensity of the burst. As a result, we could not constrain the spectral parameters of any spectrum during the 15–33 s time interval. However, our spectral analysis covers the main part of the single pulse of the light curve and excludes only the last decaying part of the light curve.

Although the B and CPL model can fit the time-resolved spectra and give consistent results (top and mid panels of Fig. 3), we note that in four out of seven spectra the B model yields an unconstrained high-energy spectral index β, suggesting that the CPL model represents the data better. The low-energy spectral index α in both cases is harder than the cooling limit, and for three out of seven spectra it also violates the optically thin synchrotron limit. The evolution of the peak energy is smooth and it decreases monotonically from $\sim$200 keV at the beginning to a few tens of keV in the final part of the burst.

The fit with a BBPL model (Fig. 3, bottom panel) gives a soft power-law index, remaining softer than $-3/2$ during the burst evolution. Overall, we note that the blackbody contribution to the total flux is around 40 per cent except for one spectrum that has a quite considerable blackbody flux (i.e. $\sim$80 per cent). The peak energy (in this case the peak of the blackbody component) is consistent, in terms of values and evolution, with that of the B and CPL model.

The time-integrated spectrum, accumulated over the 33 s duration of the burst, is well fitted by the three models although, also in this case, the B model has β unconstrained. The low-energy spectral index of the time-integrated spectrum is $\alpha = -1.26 \pm 0.14$ and the peak energy is $E_{\rm peak} = 123 \pm 36$ keV (Table 2), consistent with those reported in Table 1. The BBPL model fitted to the time-integrated spectrum gives a very soft power law ($\alpha = -2.19 \pm 0.16$) and a peak energy of the blackbody component $E_{\rm peak} \sim 137$ keV, which is consistent with the fit obtained with the CPL model.

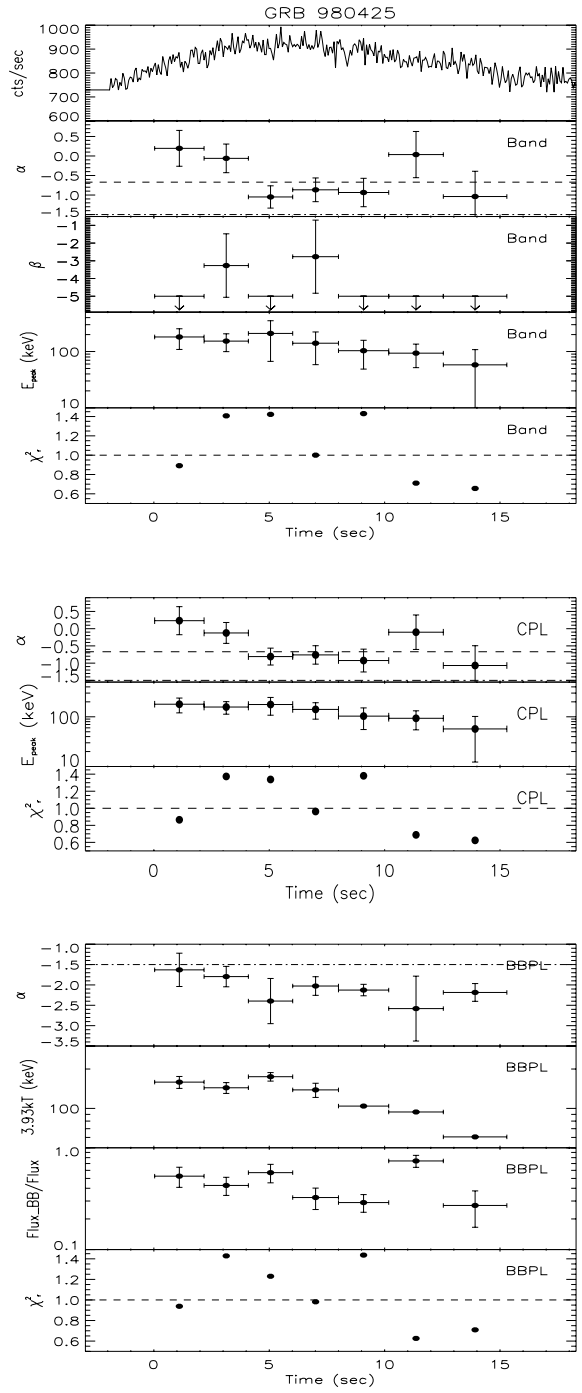

Figure 3. Spectral evolution of GRB 980425. Symbols are the same as in Fig. 1.

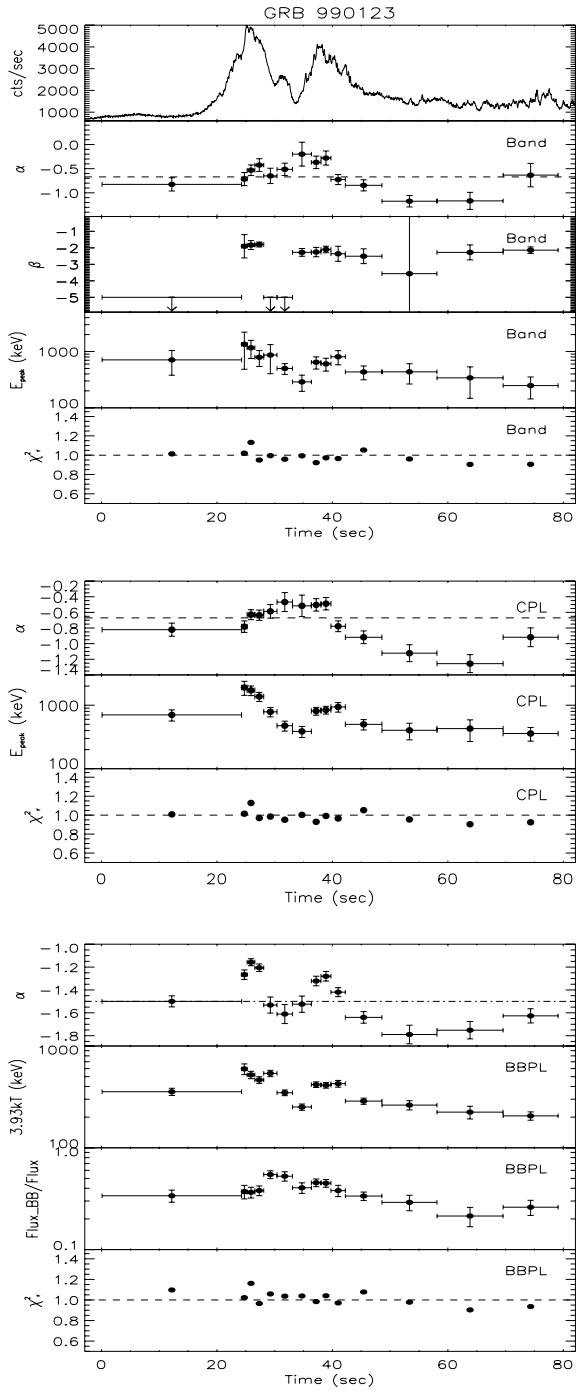

Figure 4. Spectral evolution of GRB 990123. Symbols are the same as in Fig. 1.

4.1.6 GRB 990123

GRB 990123 (BATSE trigger 7343) is a long-duration event with a very high fluence. The light curve has two major peaks and a long tail after the second peak. There is a gap in the LAD data corresponding to the beginning of the burst up to 20 s. For this reason, we used the SD data. The spectral evolution (Fig. 4) shows that the peak energy slightly precedes the light curve first peak while it tracks the second peak (see e.g. Ghirlanda et al. 2002). The low-energy spectral component is harder than the synchrotron limit during most of the two major peaks. The B and CPL models have similar time-resolved spectral parameters. The BBPL model fits the time-resolved spectra with a power-law component which is harder than the -1.5 limit. The blackbody flux is no more than 50 per cent of the total flux.

The time-integrated spectrum accumulated over $\sim$100 s (in order to include the long tail of the second peak) is fitted by both the B and the CPL model. These models give similar results: the low-energy spectral index is $\alpha = -0.85 \pm 0.04$ (B) and $\alpha = -0.9 \pm 0.03$ (CPL); the peak energy is $E_{\rm peak} \sim 605$ keV (B) and $E_{\rm peak} \sim 684$ keV (CPL). The latter values are lower than those reported in Table 1. This is

likely due to the better energy coverage of the BATSE data (with respect to the GRBM spectrum – Amati et al. 2002): the extension of the energy range up to 1800 keV allows to better determine the value of $E_{\rm peak}$.

4.1.7 GRB 990510

GRB 990510 (BATSE trigger 7560) has a light curve with two main structures (lasting 10 and 20 s, respectively) composed of several subpeaks and separated by a quiescent phase lasting ≈30 s. We could extract six spectra (distributed between 0 and 8 s) corresponding to the first set of peaks and 17 spectra (between 40 and 60 s) corresponding to the second set of peaks. Given the long quiescent phase, we separately analysed the time-averaged spectra integrated over the first and the second phase.

The time-resolved spectra are well fitted with the CPL and the B model which give similar results (see Fig. 5). The comparison of the low-energy spectral index and the peak energy between the first and the second phase shows that the spectrum of the latter is (on average) slightly softer in terms of α and harder in terms of $E_{\rm peak}$ than the former. The low-energy spectral index α is harder than the optically thin synchrotron limit for most of the first peak and is consistent with this limit during the second emission episode. $E_{\rm peak}$ rises and decays during the first peaks while it has a more regular hard-to-soft evolution during the second set of peaks.

The fit with the BBPL model (Fig. 5, bottom panels) is consistent with the behaviour observed in previous bursts. In the case of the first peak, we could not constrain the blackbody component of the BBPL model. We therefore fixed, only for the time-resolved spectra of the first peak, the blackbody temperature so that its peak corresponds to the value found by fitting the B model. In the case of the BBPL model, the power-law component is much softer than the low-energy component of the CPL model and does not violate the $-3/2$ (cooling) limit. The peak energy of the blackbody component evolves similarly to that of the CPL (or B) model and is slightly harder in the second emission phase than in the first. The blackbody component contributes at most 30 per cent of the total flux of the time-resolved spectra.

The time-integrated spectra of the first and the second set of peaks have been fitted separately (Table 2). The spectral parameters of the fit of the second peak are consistent with that reported in Table 1 obtained with the *BeppoSAX* WFC+GRBM data (Amati et al. 2002).

4.2 Inconsistency of the blackbody+power-law model with the Wide Field Camera data

The results obtained from the time-resolved analysis of the GRBs of our sample indicate that the fit with a BBPL model gives acceptable results for all bursts. This model has also the advantage, with respect to the B and the CPL model, to require a soft power-law component with a spectral index always consistent (except for GRB 990123) with a cooling particle distribution (i.e. $\alpha < -3/2$). In Fig. 6, we compare the photon index of the CPL model (which is in most cases consistent with α of the B model) to that the BBPL model. Note that the latter is always softer than the corresponding parameter of the CPL model. In the same plot, we also mark the synchrotron limits and show that the power law of the BBPL model is consistent with these limits being (except for GRB 990123) softer than $-3/2$. Also, when considering the time-integrated spectra we find that the power-law component of the BBPL model is systematically softer

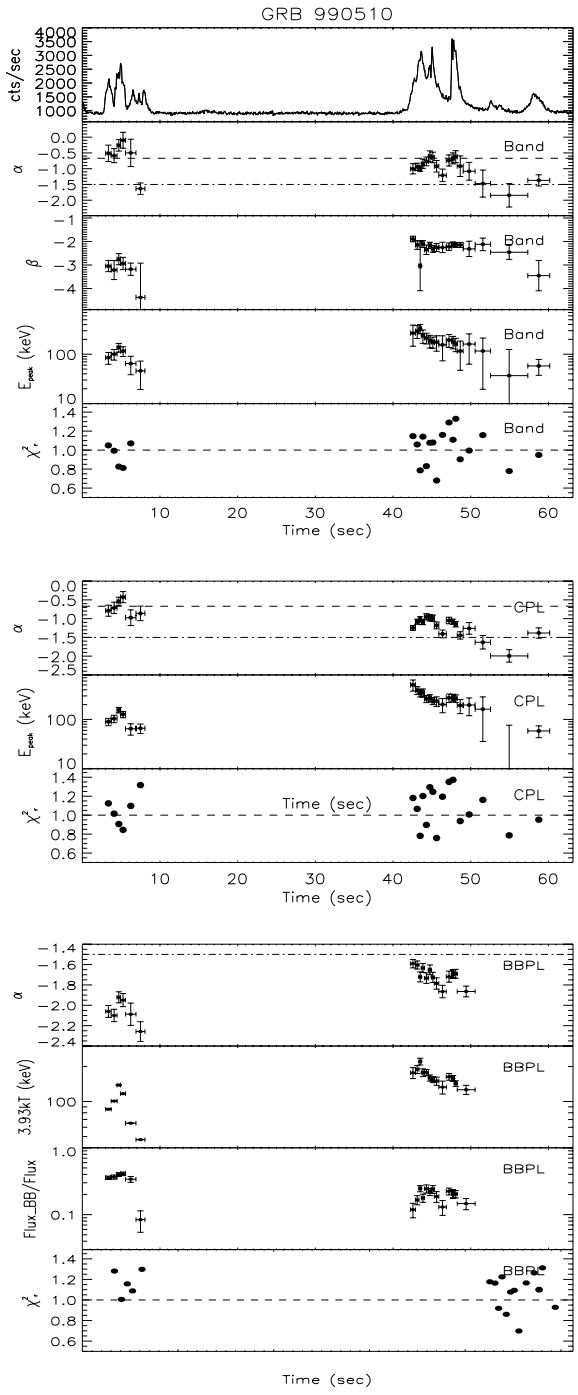

Figure 5. Spectral evolution of GRB 990510. Symbols are the same as in Fig. 1.

than the power-law components of the B or CPL model (compare Columns 7 and 3 in Table 2).

The peak energy $E_{\rm peak}$ resulting from fitting the data with the BBPL model is indeed produced by the blackbody component which substantially contributes to the total energetics, at least in the observed energy range of BATSE. This would thus favour the 'blackbody interpretation' of the spectral-energy correlation which we have summarized in Section 2.

However, these results are based on the spectral analysis of the BATSE spectra only. Although covering two orders of magnitude in

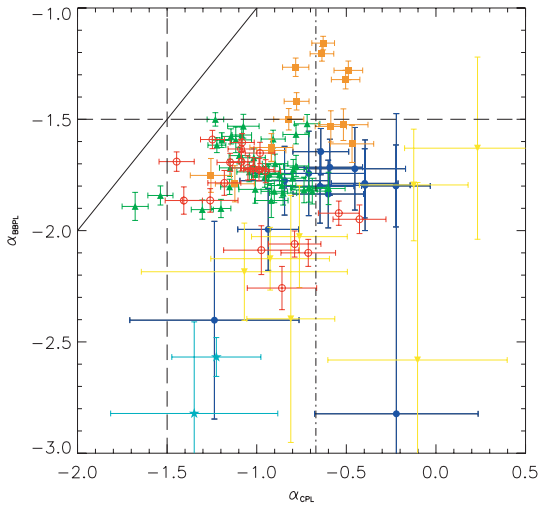

Figure 6. Comparison of the photon index of the power-law component of the BBPL model ($\alpha_{\rm BBPL}$) with the low-energy photon spectral index obtained from the CPL fit ($\alpha_{\rm CPL}$). Different symbols correspond to: 971214 (filled circles), 980326 (filled stars), 980329 (triangles), 980425 (upside-down triangles), 990123 (squares) and 990510 (open circles). The solid line represents the equality of the two spectral indices. The long-dashed line and the dot–dashed line are the synchrotron limits with and without cooling, respectively.

energy, these data do not extend below 20 keV and above 2000 keV. The low-energy limit is particularly relevant here, since for these bursts we do have the information of the low (2–28 keV) energy emission from the WFC of *BeppoSAX*. We can then compare the result of the BBPL model with the flux and spectrum observed by the WFC. Since the latter concerns the time-integrated spectrum, we should then either add the single time-resolved spectra to construct the total flux and spectrum for each burst or use the result obtained by fitting the BATSE time-integrated spectrum. In both the cases, we have to extrapolate the model to the energy range of the WFC.

As stated above, the inclusion of the blackbody component implies that the accompanying power-law component becomes soft (i.e. $\alpha < -1.5$). It is this power-law component that mainly contributes at low energies, and we find, in all cases, a strong disagreement between the extrapolated flux and spectrum of the WFC data.

This is shown in Figs 7–12, where we report the BATSE time-integrated spectrum and the WFC spectrum. In the three panels of these figures, we report the results of the fit with the three models described in Section 3, i.e. the B model, the CPL model and the composite model (BBPL). We report both the model fit to the time-integrated spectrum (solid line) to the time-resolved spectra (dotted lines) and the sum of the time-resolved model fits (dot–dashed line).

One can see that in all cases, the BBPL model strongly overpredicts the observed flux in the WFC 2–28 keV energy band, with a slope which is much softer than observed. This occurs both when we sum the time-resolved spectra and when we use the time-integrated fits. On the contrary, note the excellent agreement of the extrapolated flux and the WFC data in the case of the B and the CPL fits. To the best of our knowledge, this is the first time that a detailed comparison of the WFC *BeppoSAX* and the BATSE data is performed. We conclude that they are in excellent agreement *if the spectrum is indeed described by the B or CPL model, and that the BBPL model cannot reproduce the WFC data.*

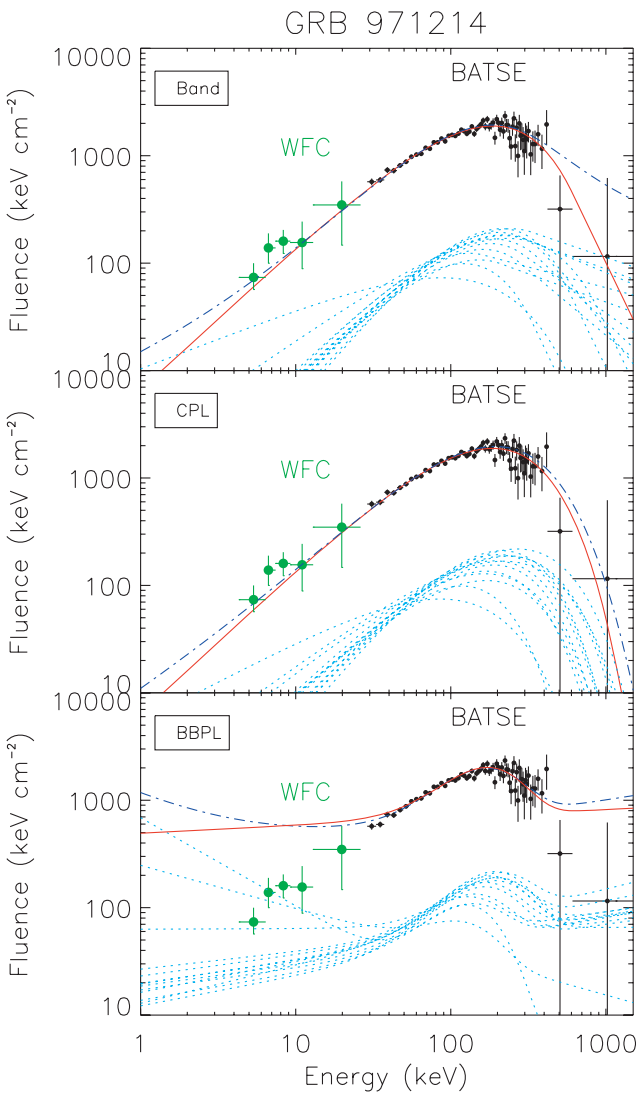

Figure 7. GRB 971214: BATSE time-integrated spectrum and WFC data (black and grey points, respectively). In the three panels, we show the spectral fits of the time-resolved spectra (dotted lines), the spectral fit of the time-integrated spectrum (solid line) and the sum of the time-resolved spectral fits (dot–dashed line). Spectral fits with the B model (top panel), CPL model (mid panel) and BBPL model (bottom panel) are shown.

We can also conclude that a fit with a blackbody only (without the power law) is never consistent with the data, even when considering spectra at the peak of the light curve or for the first phases of the emission. This is because fitting the CPL model, which can mimic a blackbody when $\alpha = 1$, always gives $\alpha < 0$.

Our analysis also shows that the blackbody component in the time-resolved spectra that we have analysed (typically with >0.1 s time resolution) does not change much during the burst. This implies that even if it were possible to perform the spectral analysis with a finer temporal resolution, it is unlikely that the time-resolved spectra are the superposition of a multitemperature blackbody.

Finally, we cannot exclude the possibility that the instantaneous spectrum is produced by a superposition of blackbody components. Indeed, this is exactly what happens in thermal or quasi-thermal Comptonization models (if the seed photons have a relatively narrow range of frequencies), where the superposition of different scattering orders (each one being blackbody like)

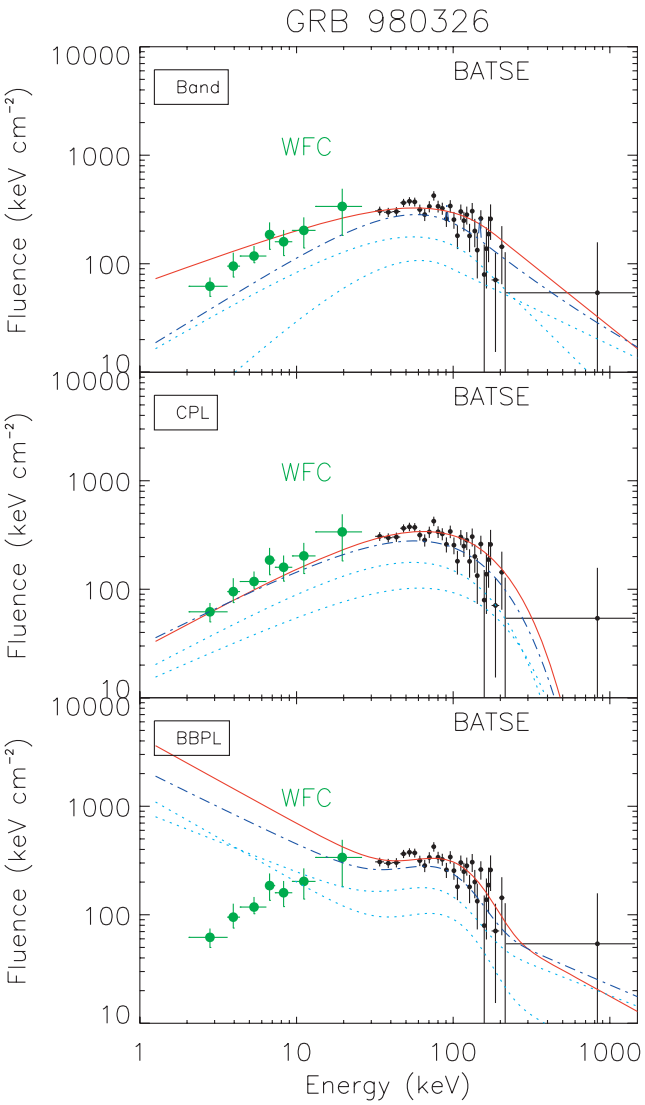

Figure 8. GRB 980326. Symbols are the same as in Fig. 7.

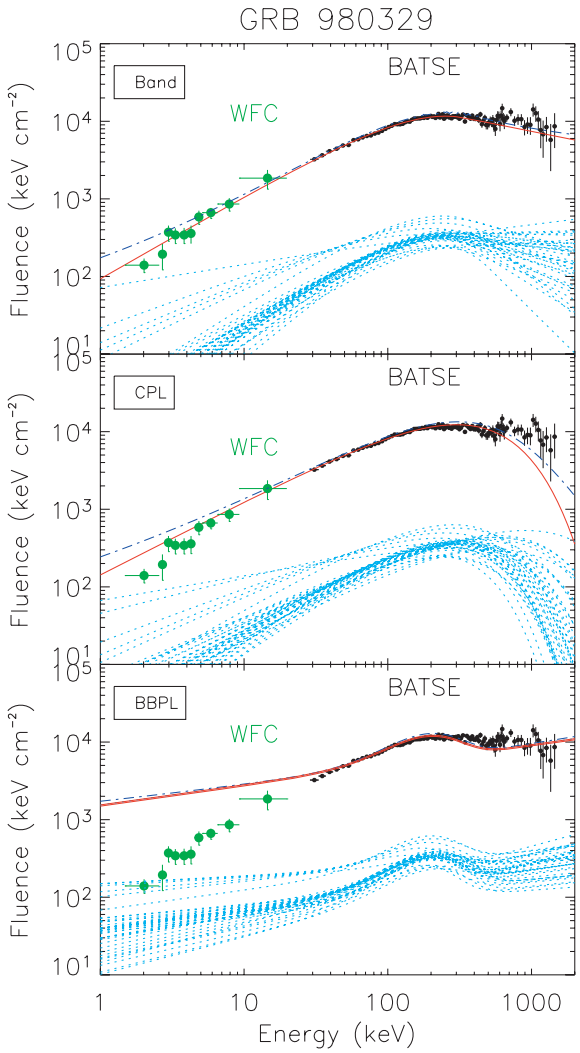

Figure 9. GRB 980329. Symbols are the same as in Fig. 7.

produces the CPL spectrum. Blackbody components produced in different (and independent) emitting regions, instead, are less likely, since some fine-tuning is required in order to produce the smooth observed spectrum.

4.2.1 Further testing the blackbody component

The existence and the relevance of a blackbody component in the spectra of our GRBs can be further tested allowing for the possibility that the real spectral model is more complicated than what we thought. We could make the BBPL model fits consistent with the WFC [2–28 keV] spectra by introducing a spectral break between the BATSE and the WFC energy ranges. This could indeed be the case if the non-thermal component is produced by an electron energy distribution with a low-energy cut-off, or if the apparently non-thermal component is instead the result of a thermal Comptonization process (e.g. Liang 1997; Liang et al. 1997; Ghisellini & Celotti 1999; Meszaros & Rees 2000). In the latter case, what we see in the WFC could be the (hard) spectrum of the seed photons, while in BATSE we may see the sum of the Comptonization spectrum and a blackbody.

We must then check if, in this case, it is possible that a blackbody is present and is responsible for a significant fraction of the total flux and for the observed $E_{\rm peak}$, without violating any observational constraint. If so, then the 'blackbody' interpretation presented in Section 2 would receive support.

However, there are severe problems with this possibility. The first is that the required break should always be at ∼30 keV (between the BATSE and the WFC energy ranges) despite the fact that our GRBs have different redshifts. This makes this possibility rather ad hoc.

The second problem comes from the following test. As stated, we should use a model composed by blackbody plus a Band spectrum. This model, unfortunately, has too many free parameters to yield strong constraints, but we can mimic it by adopting a model composed by the sum of a blackbody and CPL. The index of the latter should be thought as the low-energy index of the B model. Furthermore, since what we really put on test is the presence of a relevant blackbody, we can also fix its temperature requiring it to give the $E_{\rm peak}$ found when using the CPL (or B) model. This is because we already know that these $E_{\rm peak}$, when combined in the time-integrated spectrum, give the $E_{\rm peak}$ used for the Amati and Ghirlanda correlations.

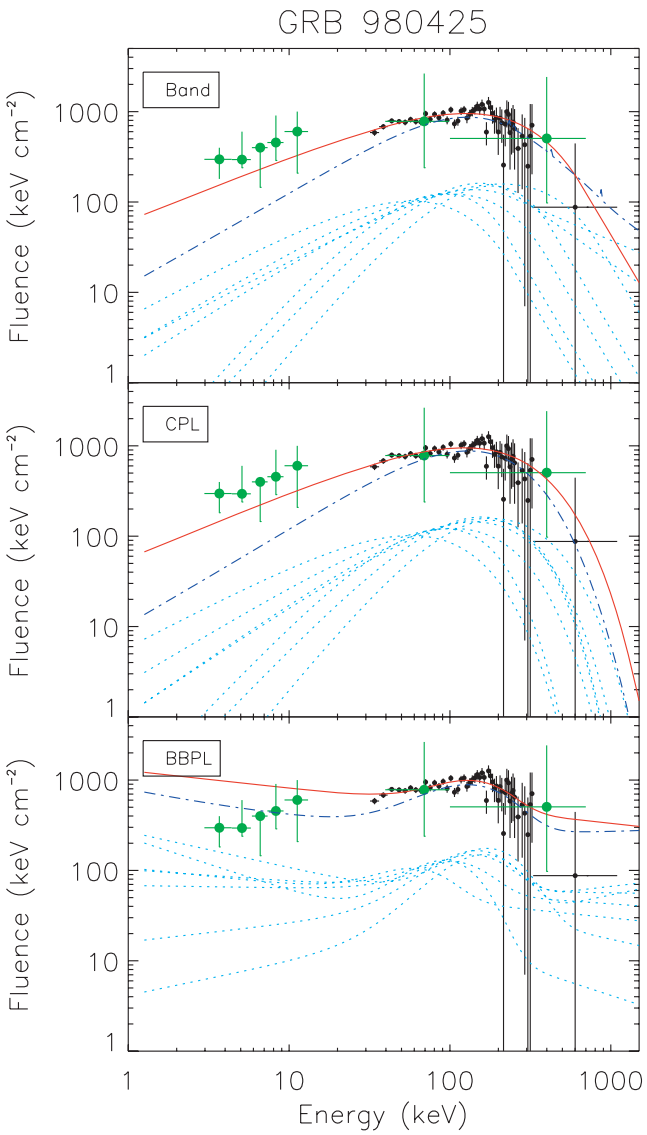

Figure 10. GRB 980425. Symbols are the same as in Fig. 7. In this case, we also show the two data points of the GRBM instrument onboard *BeppoSAX* covering the 40–700 keV energy range.

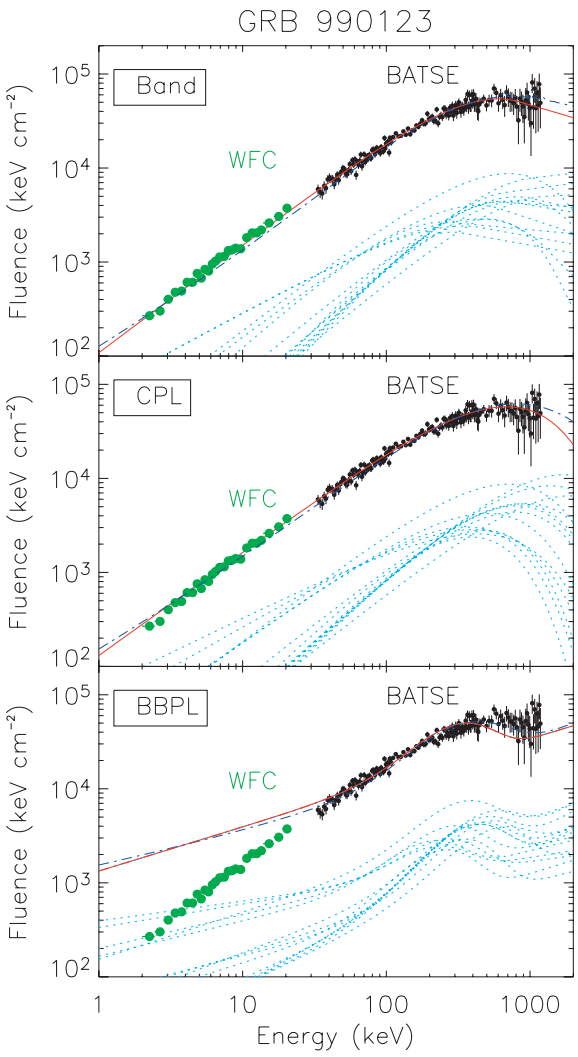

Figure 11. GRB 990123. Symbols are the same as in Fig. 7.

We thus use this blackbody+cut-off power-law (BBCPL) model:

$$N(E) = A\frac{E^2}{\exp(E/kT)-1} + BE^{\alpha}\exp\left(-\frac{E}{E_0}\right), \quad (8)$$

where kT, i.e. the blackbody characteristic temperature, is fixed so that $3.9kT = E_{\rm peak}$ (as found from the fit of the CPL model to each time-resolved spectrum). This model has the same number of free parameters of the BBPL and B model (the two normalizations, E_0 and α).

In Fig. 13, we compare the photon index found with a simple CPL model and the α of the BBCPL model described above. In the BBCPL model, the photon index of the CPL component can fit the WFC data and indeed we found it to be consistent with the values found by the fit of a simple CPL model. *Instead, the blackbody component is negligible in all these fits.*

For each time-resolved spectrum fitted with the BBCPL model, we can compute the fraction of the rest-frame bolometric flux contributed by the blackbody component. Summing up these contributions for the entire duration of each burst, we derive the contribution of the blackbody to the time-integrated flux. The values are reported in Table 2 (last column): for all the bursts this contribution is small.

We can then conclude that if a blackbody is present, with a temperature consistent with the peak of the spectrum (found by fitting the CPL model), then its flux is not relevant. Consider also that this spectral model is not required by the data, which are instead well described by the simpler CPL (or B) model. In this sense, what we found is an *upper limit* to the possible contribution of a blackbody to the total flux.

5 SUMMARY OF RESULTS

We have analysed the spectra of seven GRBs detected by BATSE with measured redshift and for which also the *BeppoSAX* WFC spectrum has been published (Amati et al. 2002). We analysed both the time-resolved and the time-integrated spectrum with three models: the B model, a CPL model and a BBPL model. For a further test of the importance of a possible blackbody component, we have also used the sum of a BBCPL model. The comparison of the spectral parameters and the analysis of the spectral evolution have shown that:

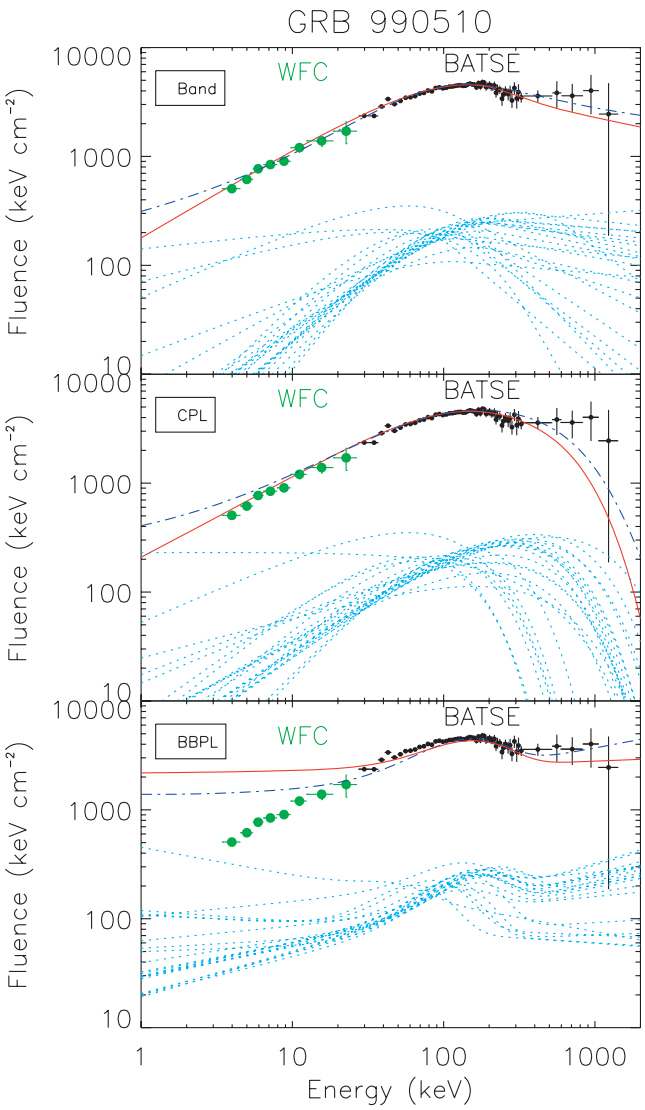

Figure 12. GRB 990510. Symbols are the same as in Fig. 7.

(i) the time-resolved spectra could be reasonably fitted with all models. The spectral parameters of the B and CPL model agree within their uncertainties;

(ii) in all our GRBs the spectral slope of the low-energy component of the B or CPL model violates both the optically thin synchrotron limit with (−1.5) or without (−0.67) radiative cooling;

(iii) the values of $\alpha < 0$ found from the fit of the CPL model exclude the possibility that a single-blackbody model can fit these spectra (as the blackbody coincides with the CPL model only for $\alpha = 1$);

(iv) the power-law slope of the BBPL model is softer than the corresponding parameter of the B or CPL model. In most GRBs (except GRB 990123), this component is softer than the optically thin synchrotron limit with cooling (−1.5) and softens as time goes by;

(v) the peak energies of the blackbody component of the BBPL model found here are similar to the values found for a few other bursts analysed with the BBPL model (Ryde 2005) or with a single blackbody component (GCG03);

(vi) the blackbody flux (in the BBPL model) is no more than 50 per cent of the total flux and it changes with time. In these bursts, the blackbody does not dominate the initial emission phase as was the case of the few GRBs analysed by GCG03;

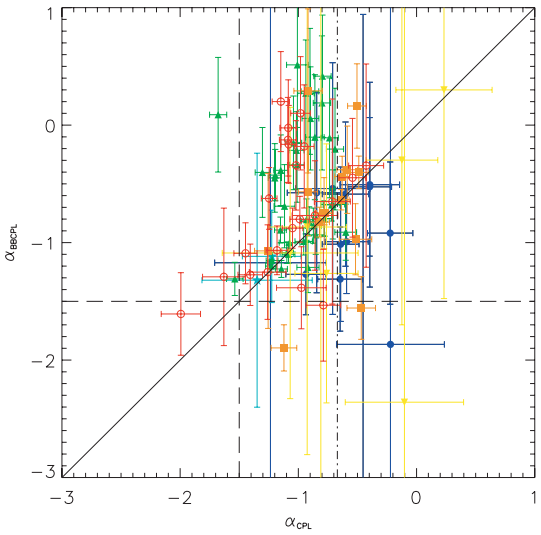

Figure 13. Comparison of the spectral photon index of the CPL model (α_{CPL}) with the photon index obtained from the fit of a CPL plus a blackbody with the peak of the blackbody fixed to the values found from the fit of a simple CPL model. Symbols are as in Fig. 6.

(vii) the soft power-law spectra found using the BBPL model imply a relatively large flux of the spectrum extrapolated at lower energies. This extrapolation is inconsistent with the WFC data and spectra (Figs 7–12);

(viii) the time-integrated spectral fit and the sum of the time-resolved spectral fits with either the B and CPL model are consistent with the WFC spectrum in terms of both flux and slope;

(ix) fitting the BATSE spectra with the BBCPL model results in a CPL component whose extrapolation to the WFC energy range is consistent with the observed spectrum in terms of flux and slope. In this case, however, the blackbody flux is not significant.

6 CONCLUSIONS

The most important result of this work is the assessment of the importance of a blackbody component in the spectra of GRBs. For the GRBs analysed here, we find that it cannot be, at the same time, responsible for the peak (in νF_ν) of the spectrum and for its total energetics. We could reach this conclusion by analysing the time-resolved spectra of those GRBs detected by BATSE and by the WFC of *BeppoSAX*, therefore using the energy range between 2 keV and 2 MeV. We also find that the BATSE data, fitted by a CPL or by the B model, are entirely consistent with the WFC data.

These findings bear important consequences on the interpretation of the peak-energy correlations (including the Amati, the Ghirlanda and the Firmani correlations) put forward recently by Thompson (2006) and by Thompson, Meszaros & Rees (2007). This interpretation requires that the blackbody component is responsible for the peak energy $E_{\rm peak}$ and for a significant fraction of the bolometric emitted energy. Note that, since the temperature of the blackbody component may vary in time, the time-integrated spectrum may not be particularly revealing of the blackbody presence, making a time-resolved analysis mandatory.

One may argue that the spectrum is even more complex than what we thought, having an additional break and becoming harder at low energies. Such a break is expected if the spectrum is due to

a thermal photospheric emission (the blackbody component) superimposed to non-thermal emission due to some dissipative mechanism (Meszaros & Rees 2000). An alternative possibility is that the observed spectra result from multiple Compton up-scattering of soft seed photons (e.g. Ghisellini & Celotti 1999; Thompson 2006). In such a case, a break is expected between the (possibly) hard seed photon spectrum and the beginning of the Comptonized spectrum.

But even by fitting the spectra with a more complex model allowing for this break, we found that the blackbody component is not relevant. This, together with the rather ad hoc requirement of having a break always at 30 keV (observed) irrespective of the different redshifts of our GRBs, leads us to conclude that the presence of relevant blackbody in the spectrum of our GRBs is to be excluded. This in turn makes more problematic (and mysterious) the interpretation of the spectral-energy correlation in long GRBs.

ACKNOWLEDGMENTS

We thank Annalisa Celotti for discussion and a PRIN-INAF 2005 grant for funding. We are grateful to the referee for her/his comments. This research has made use of data obtained through the High Energy Astrophysics Science Archive Research Centre Online Service, provided by the NASA/Goddard Space Flight Centre.

REFERENCES

Amati L., Frontera F., Tavani M. et al., 2002, A&A, 390, 81
Band D., Matheson J., Ford L. et al., 1993, ApJ, 413, 281
Barraud C., Olive J.-F., Lestrade J. P. et al., 2003, A&A, 400, 1021
Bloom J. S., Kulkarni S. R., Djorgovski S. G. et al., 1999, Nat, 401, 453
Bosnjak Z., Celotti A., Ghirlanda G., 2006, MNRAS, 370, L33
Crider A., Liang E. P., Smith I. A., 1997, ApJ, 479, L39
Daigne F., Mochkovitch R., 2000, A&A, 358, 1157
Firmani C., Ghisellini G., Avila–Reese V., Ghirlanda G., 2006, MNRAS, 370, 185
Ford L., 1993, A Guide to the Spectroscopic Oriented Analysis Routines, version 2.1
Ford L. A., Band D. L., Matteson J. L. et al., 1995, ApJ, 439, 307
Frontera F., Amati L., Costa E., 2000, ApJS, 127, 59
Galama T., Vreeswijk P. M., van Paradijs J. et al., 1998, Nat, 395, 670
Ghirlanda G., Celotti A., Ghisellini G., 2002, A&A, 393, 409
Ghirlanda G., Celotti A., Ghisellini G., 2003, A&A, 406, 879 (GCG03)
Ghirlanda G., Ghisellini G., Lazzati D., 2004, ApJ, 616, 331 (GGL04)
Ghirlanda G., Ghisellini G., Firmani C., Celotti A., Bosnjak Z., 2005, MNRAS, 360, L45
Ghirlanda G., Nava L., Ghisellini G., Firmani C., 2007, A&A, 466, 127
Ghisellini G., Celotti A., 1999, ApJ, 511, L93
Ghisellini G., Ghirlanda G., Mereghetti S., Bosnjak Z., Tavecchio F., Firmani C., 2006, MNRAS, 372, 1699
Golenetskii S. V., Mazets E. P., Aptekar R. L., Ilinskii V. N., 1983, Nat, 306, 451
Jimenez R., Band D., Piran T., 2001, ApJ, 561, 171
Kaneko Y., Preece R. D., Briggs M. S., Paciesas W. S., Meegan C. A., Band D. L., 2006, ApJS, 166, 298
Katz J. I., 1994, ApJ, 432, L107
Kulkarni S., Djorgoski S. G., Ramaprakash A. N. et al., 1998, Nat, 393, 35
Kulkarni S., Djorgovski S. G., Odewahn S. C. et al., 1999, Nat, 398, 389
Lamb D., Castander F. J., Reichart D. E., 1999, A&AS, 138, 479
Liang E. P., 1997, ApJ, 491, L15
Liang E., Zhang B., 2005, ApJ, 633, L611
Liang E. P., Kusunose M., Smith I., Crider A., 1997, ApJ, 479, L35
Medvedev M. V., 2000, ApJ, 540, 704
Meszaros P., Rees M. J., 2000, ApJ, 530, 292
Metzger M. R., Djorgovski S. G., Kulkarni S. R., Steidel C. C., Adelberger K. L., Frail D. A., Costa E., Frontera F., 1997, Nat, 387, 878
Pe'er A., Meszeros P., Rees M. J., 2006, ApJ, 642, 995
Pian E. et al., 2000, ApJ, 536, 778
Preece R. D., 1997, ApJ, 496, 849
Preece R. D., Briggs M. S., Malozzi R. S., Pendleton G. N., Paciesas W. S., Band D. L., 2000, ApJS, 126, 19
Rees M. J., Meszaros P., 2005, ApJ, 628, 847
Ryde F., 2004, ApJ, 614, 827
Ryde F., 2005, ApJ, 625, L95
Ryde F., Svensson R., 2000, ApJ, 529, L13
Tavani M., 1996, ApJ, 466, 768
Thompson C., 2006, ApJ, 651, 333
Thompson C., Meszaros P., Rees M. J., 2007, ApJ, in press (astro-ph/0608282)
Vreeswijk P. M., Fruchter A., Kaper L. et al., 2001, ApJ, 546, 672
Yonetoku D., Murakami T., Nakamura T., Yamazaki R., Inoue A. K., Ioka K., 2004, ApJ, 609, 935

This paper has been typeset from a TEX/LATEX file prepared by the author.